Endo or Exo? Structures of Gas Phase Alkali Metal Cation/Aromatic Half-Belt Complexes

Yanyang Chen,[a] Yasaman Jami-Alahmadi,[a] Kiran Sagar Unikela,[a] Graham J. Bodwell,*[a] and Travis D. Fridgen*[a]

Abstract: 1,1,9,9-Tetramethyl[9](2,11)teropyrenophane (TM9TP), a belt-shaped molecule, has a sizable cavity that molecules or ions could occupy. In this study, the question of whether TM9TP forms gas phase ion-molecule complexes with metal cations (K^+, Rb^+, Cs^+) situated inside or outside the TM9TP cavity was addressed using both experimental and computational methods. Complexes were trapped in a Fourier transform ion cyclotron resonance mass spectrometer and their structures were explored by some novel physical chemistry/mass spectrometry methods. Blackbody infrared radiative dissociation kinetics reveal two populations of ions, a fast dissociating fraction and a persistent fraction. Infrared multiphoton dissociation spectra (vibrational spectra) provide very strong evidence that the most abundant population is a complex where the metal cation is inside the TM9TP cavity, *endo*-TM9TP. Red-shifted C-H stretching bands revealed in the gas-phase vibrational spectra of these ionic complexes show that there is an interaction between the metal cation and a bridge C-H bond due to the cation sitting inside the cavity of TM9TP. B3LYP/6-31+G(d,p) calculations showed the *endo* complexes to be the lowest in energy and about 50 kJ mol^{-1} more thermodynamically stable and more than 100 kJ mol^{-1} kinetically more stable than the *exo* complexes.

Introduction

The pioneering work of the 1987 Nobel laureates[1] Pederson,[2] Lehn[3] and Cram[4] laid much of the groundwork for modern supramolecular chemistry.[5] A central theme in this area is the formation of host-guest complexes, whereby organic molecules with a cavity of some description can accommodate a guest molecule and/or ion. Not only the shape and size of the cavity, but a variety of non-covalent interactions[6] such as hydrogen bonding, electrostatic effects, van der Waals forces, hydrophobic forces, π-π stacking interactions, and cation-π interactions contribute to provision of a welcoming and selective environment for guests.[7]

Cyclophanes, which can be loosely defined as assemblies of aromatic units and bridging aliphatic units,[8] have played an important role in the development of host-guest chemistry.[9] From a structural perspective, the aromatic units[8] of a host cyclophane not only provide a degree of rigidity that contributes to the formation of a non-collapsible cavity,[10] but also offer π electron clouds that are able to interact with cations, anions and neutral molecules.[11] On the other hand, the bridges provide a degree of flexibility that enables the host some latitude to adjust the dimensions of its cavity in response to a guest. For example, cyclophane **1** (5 aromatic units, 6 bridges; Scheme 1) has a cavity that enables it to serve as a host for neutral molecules and anions such as acetone, $Cl^-\cdots H_2O$, and I^-.[12] On the other hand, duplexiphane (**2**) was found to be a suitable host for Ag^+.[13]

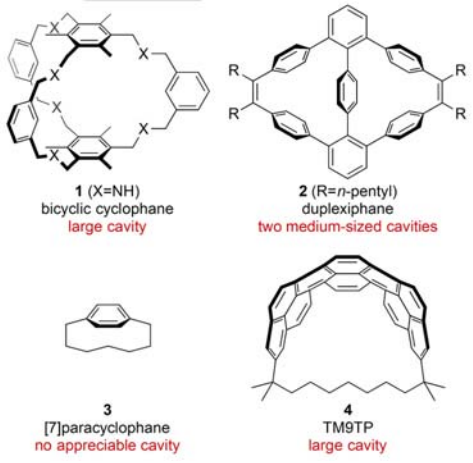

Scheme 1. Homoditopic hexamino bicyclic cyclophane (**1**), duplexiphane (**2**), [7]paracyclophane (**3**), and TM9TP (**4**).

Until now, all the cyclophanes that have been employed in the context of host-guest chemistry have had more than one aromatic unit and more than one bridge, e.g. **1**. In other words, no [*n*]cyclophane (1 aromatic unit and 1 bridge) has ever seen application in this area. This is simply because the aromatic systems (usually benzene) that have been used to construct host cyclophanes are far too small to be able to form [*n*]cyclophanes with an appropriately-sized and sufficiently shape-persistent cavity. For example, [7]paracyclophane (**3**) has no appreciable cavity. Substantially larger [*n*]paracyclophanes can have significant cavities, but lack shape-persistence. Upon moving to larger aromatic systems, there are very few examples of [*n*]cyclophanes with arenes larger than pyrene.[8] Indeed, a variety of [*n*](2,7)pyrenophanes have been synthesized and characterized crystallographically, but none of them has anything more than a very small cavity.[14]

[a] Department of Chemistry
Memorial University of Newfoundland
Memorial University, St. John's, NL, A1B 3X7, Canada

* to whom all correspondence should be addressed at:
tfridgen@mun.ca or gbodwell@mun.ca

Supporting information for this article is given via a link at the end of the document.((Please delete this text if not appropriate))

Teropyrene is the largest aromatic system to have been incorporated into a [*n*]cyclophane.[15] A short series, of 1,1,*n*,*n*-tetramethyl[*n*](2,11)teropyrenophanes was recently reported, the highest homologue of which is 1,1,9,9-tetramethyl[9](2,11)teropyrenophane (**4**, TM9TP).[15b] TM9TP has a relatively large, roughly semicircular-shaped cavity. A distance of 9.80 Å between the two bridgehead carbon atoms was determined using X-ray crystallography.[15b] As such, a range of molecules or ions could conceivably be hosted by TM9TP.

Host-guest complexes of cyclophanes have been studied almost exclusively in solution.[16] However, in order to explore the fundamental nature and extent of non-covalent interactions between a host and its guest, the effects of solvents should be excluded. This can be accomplished using gas-phase analytical methods. Although mass spectrometry (MS) used to be an unsuitable method for the study of non-covalent complexes, the development of soft ionization techniques has enabled nondestructive ionization of weakly-bound complexes. Consequently, MS investigation of high molecular weight molecules and their non-covalent interactions with molecules and ions has become feasible.[17] Mass spectrometry has been used to investigate the interaction between halogenated dodecaborate dianions (*ie*. $B_{12}Cl_{12}^{2-}$) with non-polar aromatic organic host molecules.[18] Collision induced dissociation of these ions required excitation energies approaching those used to dissociate covalent bonds. The self-assembly of these complexes were explained to be driven by strong dispersion interactions. Infrared multiphoton dissociation (IRMPD) spectroscopy has also been used to determine that crown-ether molecules bind strongly to ions such as H_3O^+ and NH_4^+,[19] diatomic cations such as Zn^{2+} and Cd^{2+},[20] and alkali metal cations.[21] For the alkali metal cations, a size dependence was observed in complex structures where the larger cations sit above the crown ether whereas the crown ether folds to encapsulate the smaller metal cations. We report here the formation and study of gas-phase ion-molecule complexes of TM9TP with the alkali cations, K^+, Rb^+, and Cs^+ using Fourier transform ion cyclotron resonance (FT-ICR) MS in conjunction with sustained off-resonance irradiation collision-induced dissociation (SORI-CID), blackbody infrared radiative dissociation (BIRD) kinetics, and IRMPD spectroscopy.

Results and Discussion

In Figure 1 the SORI-CID mass spectra of $K(TM9TP)^+$, *m/z* 669; $Rb(TM9TP)^+$, *m/z* 715; and $Cs(TM9TP)^+$, *m/z* 763, are displayed. These complexes readily dissociate upon collisional activation by losing only the TM9TP, leaving the bare metal cations K^+, Rb^+, and Cs^+ at *m/z* 39, 85, or 133, respectively.

Relative to SORI-CID, BIRD can be considered a very soft activation technique. Ionic complexes are trapped and stored in the ICR cell (~10^{-10} mbar) and absorb a single ambient blackbody infrared photon from the ICR vacuum chamber. If the complexes are weakly bound, those at the top of the Boltzmann internal energy distribution are observed to dissociate.[22] Since the activation process involves absorption of a photon, the observed kinetics are expected to be first order as in Eq. 1 with I_t and I_0

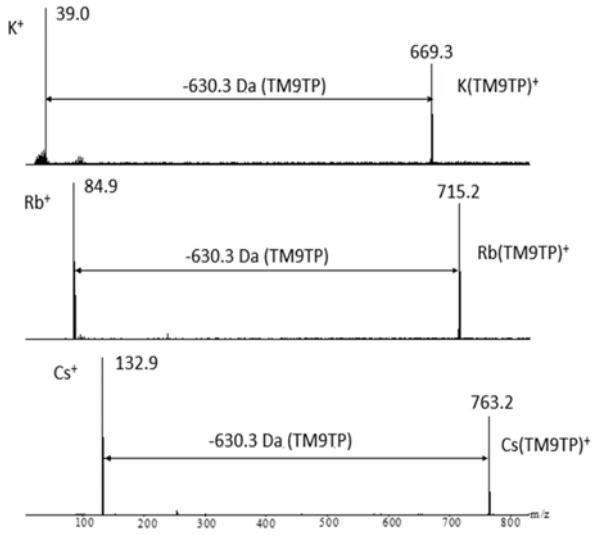

Figure 1. SORI-CID mass spectra of potassiated, rubidiated, and cesiated TM9TP complexes.

being the time dependent and initial precursor ion intensities, respectively, *k* is the first order rate constant and *t* is time.

$$I_t = I_0 e^{-kt} \quad (1)$$

In Figure 2 the time dependencies of the parent complex ions and their dissociation products (BIRD plots) are presented. It is apparent from the BIRD plots (Fig. 2) that the ion dissociation is not observed to be first order. In fact, the decay can be fitted to a biexponential, two first order dissociations:

$$I_{A,t} + I_{B,t} = I_{A,0} e^{-k_A t} + I_{B,0} e^{-k_B t} \quad (2)$$

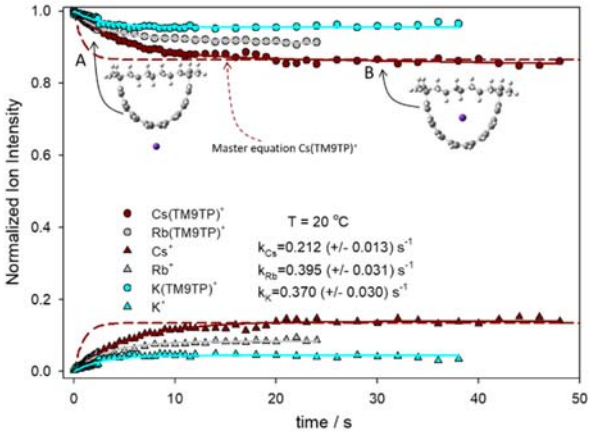

Figure 2. BIRD kinetics plots for potassiated, rubidiated, and cesiated TM9TP complexes.

suggesting two distinct populations of ions—one which is weakly bound (A) and undergoes fast BIRD kinetics and a second, significantly more persistent, population of ions (B) which is relatively more strongly bound and is actually not observed to dissociate on the time frame of the experiments, ie. k_B, the first order dissociation rate constant is essentially 0 s^{-1}. For the experiments shown, population A consists of between 5 and 15% of the mixture, depending on the cation. It is likely that initially the percentage of population A is larger, but that many of them decompose *en route* to the ICR cell from the ion source. It is tantalizing to surmise that populations A and B might be the *exo*-M(TM9TP)$^+$ and *endo*-M(TM9TP)$^+$ complexes, respectively, as shown in Figure 2, but that is merely conjecture at this point.

Electronic structure calculations were conducted and a potential energy diagram for the Rb(TM9TP)$^+$ complex is shown in Figure 3. It was determined that *exo*-Rb(TM9TP)$^+$ is significantly higher in energy (63 kJ mol^{-1}) than *endo*-Rb(TM9TP)$^+$, consistent with two populations of ions observed in the BIRD experiments. Furthermore, the *endo* and *exo* complexes are separated by a significant barrier.

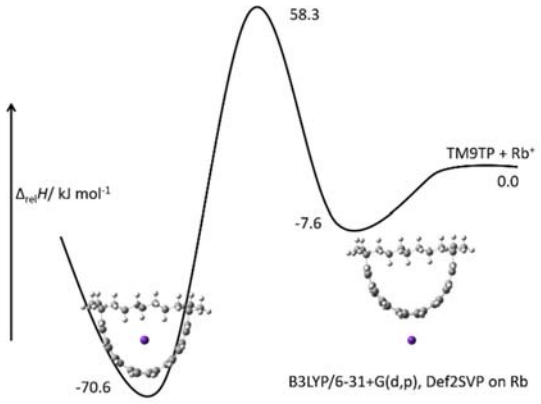

Figure 3. B3LYP/6-31+G(d,p), Def2SVP on Rb, computed 298 K enthalpy diagram for the dissociation of *endo*-Rb(TM9TP)$^+$.

To dissociate, *exo*-Rb(TM9TP)$^+$ simply loses TM9TP at a cost of merely 7.6 kJ mol^{-1}. However, the lowest energy route to dissociation for *endo*-Rb(TM9TP)$^+$ is through the barrier to the *exo* complex as shown in Fig. 3, with an activation enthalpy computed to be almost 130.0 kJ mol^{-1}. The results of these calculations are summarized in Table 1. To confirm the lowest-energy dissociation pathway, a relaxed potential energy scan was also conducted beginning with *endo*-Rb(TM9TP)$^+$ and moving the ion outward from its lowest energy position in the centre of the TM9TP molecule and perpendicular to the plane containing the alkyl bridge. During these potential energy scan calculations, the TM9TP molecule itself was frozen but the position of the ion with respect to the TM9TP was relaxed and allowed to optimize independently of TM9TP except for the fixed distance from the centre during each step of the calculation. The results of the scan are provided in Figure S1. These calculations show that the *endo*-Rb(TM9TP)$^+$ cation prefers to interact with the aromatic π electrons while dissociating and isomerizes from the *endo* to the *exo* complex prior to dissociation. This makes sense since the cation would be expected to be stabilized by the large electron density of the π system, rather than dissociating through a complex where the cation is interacting with aliphatic C-H groups.

The red dashed lines in Figure 2 are the master equation simulated BIRD dissociation plots for a population of ions containing 86.5% *endo*-Cs(TM9TP)$^+$ and 13.5% *exo*-Cs(TM9TP)$^+$ which were determined experimentally. The BIRD dissociation rate constants computed using the master equation were 4 x 10^{-7} s^{-1} for *endo*-Cs(TM9TP)$^+$ and 1.1 s^{-1} for *exo*-Cs(TM9TP)$^+$ using dissociation energies of 1.3 and 0.1 eV, respectively, for a neutral transition state (A values of between 10^{16} – 10^{14} or $\Delta S^{\neq}$ values of between 50 and 10 J K^{-1} mol^{-1}). It is clear that *endo*-Cs(TM9TP)$^+$, due to its much higher binding energy does not observably dissociate on the timescale of these experiments. Using the master equation modeling a larger dissociation rate constant is computed than observed experimentally (0.2 s^{-1}) for *exo*-Cs(TM9TP)$^+$, but still less than an order of magnitude difference. These kinetic modelling results agree with the hypothesis that the fast dissociating population is *exo*-Cs(TM9TP)$^+$ and the persistent population is *endo*-Cs(TM9TP)$^+$. The very weakly-bound *exo* complexes dissociate rapidly, on the timescale that can be observed in the BIRD experiments. However, the more strongly bound *endo* complex, requiring 130 kJ mol^{-1} to reach the threshold for dissociation, persists and is not observed to dissociate on the timeframe of these experiments. It is not unreasonable to expect such strongly-bound ions as the *endo* M(TMPTP)$^+$ complexes to

Table 1. Computed potential energy surface for the dissociation of M(TM9TP)$^+$. Values are relative 298 K enthalpies computed using B3LYPD3 (and CAM-B3LYP) with 6-31+G(d,p) basis on C and H, and def2-SVP basis on metal atoms.

Species	M = K	M = Rb		M = Cs
TM9TP$^+$	0.0	0.0	(0.0)	0.0
exo-M(TM9TP)$^+$	-18.0	-7.6	(5.9)	-13.7
TS-*exo*-*endo*	56.3	58.3		62.2
endo-M(TM9TP)$^+$	-74.3	-70.6	(-57.6)	-68.5

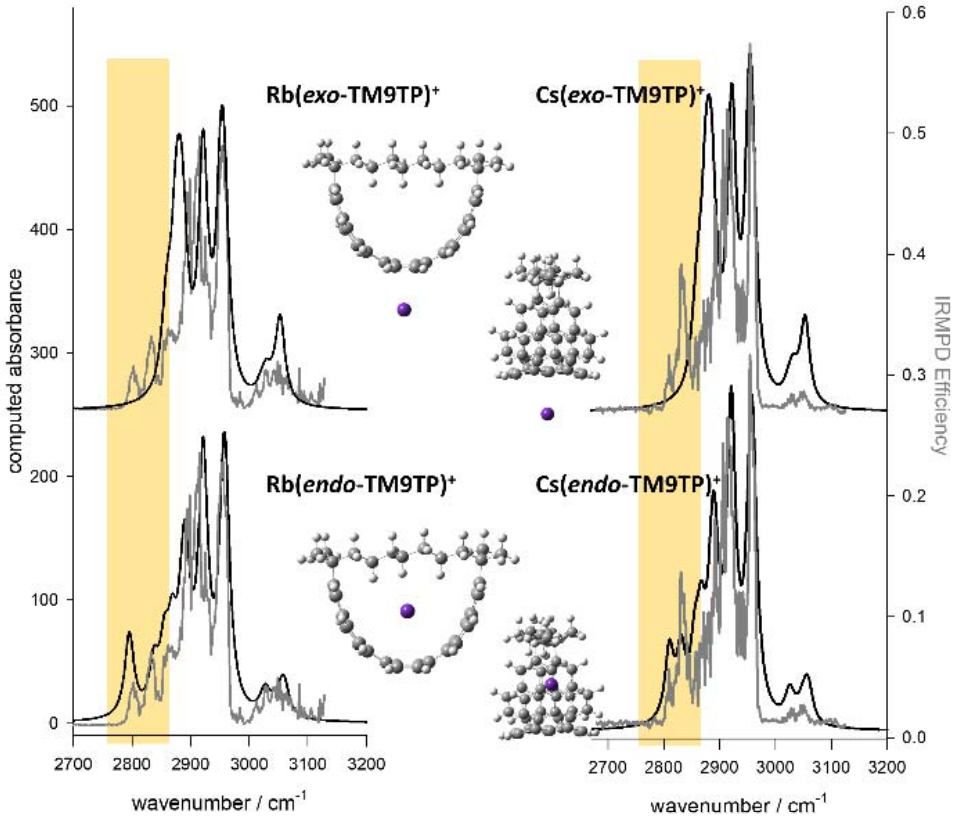

Figure 4. Comparison of the IRMPD spectra (grey traces) and computed spectra (black traces) for the $Rb(TM9TP)^+$ (left) and $Cs(TM9TP)^+$ (right) complexes in the exo (top) and *endo* (bottom) configurations.

not dissociate strongly under BIRD conditions. For example the BIRD dissociation rate constants for complexes such as $(dimethylether)_3(water)H^+$ and $(water)_4H^+$ were determined to be $9.5x10^{-2}$ and $4.6x10^{-3}$ s^{-1}, respectively,[23] with binding energies of 71[24] and 73[25] kJ mol^{-1}, respectively. However, in these cases, the complexes have strongly IR-absorbing functional groups whereas the endo $M(TM9TP)^+$ complexes have only aliphatic and aromatic C-C and C-H groups which have far less intense IR absorptions. A comparison of the computed IR spectra for endo-$Rb(TM9TP)^+$ and $(H_2O)_4H^+$ is provided in Figure S4 and shows that the water complex is far more strongly absorbing in the IR region.

The frequency calculations for the *endo* complexes revealed red-shifted C-H stretching vibrations, with respect to the *exo* complexes (see black traces in Figures 4 and S3, red shifted bands centred around 2800 cm^{-1}) such that it was anticipated that IRMPD spectroscopy (a form of vibrational spectroscopy for gaseous ions)[26] might be useful to distinguish between the *endo* and *exo* complexes.

The experimental IRMPD spectra of all three complexes are compared in Figure S2 (in Figure 4, the spectra for the Rb^+ and Cs^+ complexes are shown (grey traces). The spectra contain absorptions between 3000 and 3100 cm^{-1} which correspond to the aromatic C(sp^2)–H stretching vibrations as well as strong, sharp absorptions between 2825 and 2950 cm^{-1} due to the C(sp^3)–H bonds of the aliphatic bridge (see Figure S2A for a comparison of all three spectra). Most interestingly, there are sharp absorptions observed below 2850 cm^{-1}. These red-shifted C-H stretches are assigned to the bridge C(sp^3)–H bonds that are interacting with the K^+, Rb^+, and Cs^+ ions. Due to the C–H--M^+ interaction, the C–H bond is apparently weakened slightly; similar to the weakening of a hydrogen bonded O–H or N–H stretch. This weakening, in turn, causes a significant and clearly measurable red shift in the observed wavenumber position of the stretching vibration. The most red-shifted C-H stretch will be discussed further below.

The experimental IRMPD spectra (grey traces) in Figure 4 for $Rb(TM9TP)^+$ and $Cs(TM9TP)^+$ and in Figure S2 for $K(TM9TP)^+$ are compared to the computed IR spectra for the *endo* and *exo* complexes. The computed IR spectra for the *endo* complexes, in fact, agree very well with the experimental IRMPD spectra, including reproducing the red shifted C–H stretches. These bands below 2850 cm^{-1} are not predicted for the *exo* complexes.

The most red-shifted absorption belongs to the C-H stretch of the centre-most carbon in the bridge. It is also interesting to compare the position of this feature between the three different complexes. The band position changes from 2786 cm^{-1} in $K(TM9TP)^+$ to 2803 and 2810 cm^{-1} for the $Rb(TM9TP)^+$ and $Cs(TM9TP)^+$ complexes, respectively—the smaller, more densely-charged K^+ interacting with this bridge C-H causes the strongest red shift, followed by Rb^+ and Cs^+. This trend is expected if one considers the smaller, more densely charged K^+ interacts more strongly with the C-H bond, weakening it more with respect to Rb^+ and Cs^+ and causing a stronger red-shift. The position of that most red-shifted C-H stretch is plotted against the

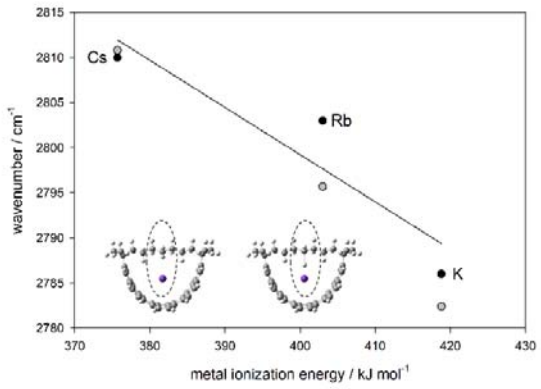

Figure 5. A plot of the computed (grey circles) and observed (black circles) central bridge C-H stretch (see inset structures) positions vs the ionization energy of the metal.

ionization energy of the metal in Figure 5 and an obvious inverse relationship is seen. Trends such as this, between the wavenumber position of a vibrational mode when it is interacting with another species have been seen before. For example, the hydrogen-bonded O-H^+-O stretch for mixed protonated *dimers* was found to be linearly dependent upon the difference in proton affinity between the two monomers.[27] The position of that band predicted by the electronic structure calculations also shows this trend providing more evidence that the complex observed—the persistent population—is the endo $M(TM9TP)^+$.

The IRMPD spectroscopic data presented here is the first direct evidence for *endo*-ion-molecule complexes in the gas phase, where the host is a non-polar molecule, and shows that the potassium, rubidium, and caesium cations sit inside the TM9TP cavity. The BIRD data clearly shows that two populations of ions are produced. This work shows that the persistent population is the *endo* complex. We can only speculate that population A, the fast-dissociating complex is the weakly-bound *exo* complex where the ion sits outside the cavity, bound to the outer π electron system.

Conclusions

Blackbody infrared radiative dissociation experiments revealed two populations of ions for K^+, Rb^+ and Cs^+ complexes with TM9TP, an aromatic half-belt. One population dissociated readily in the ICR cell while the other population persisted for very long times such that no BIRD was even observed. Red-shifted aliphatic C-H stretching absorptions observed in the IRMPD spectra of the persistent population revealed it to be the *endo* complex where the metal cation was inside *(wearing)* the aromatic half-belt. Calculations of the potential energy surface for these ions are consistent with the BIRD active population being the *exo* complexes with a very low dissociation threshold energy while the *endo* complex has a much higher dissociation threshold energy and most likely dissociates through the *exo* complex.

Experimental Section

Experimental: All experiments were performed using a Bruker ApexQe 7 FT-ICR mass spectrometer in the Laboratory for the Study of Structures, Energetics, and Reactions of Gas-Phase Ions[26a, 26c] at Memorial University. The TM9TP used in these experiments was synthesized using a recently reported gram-scale synthesis.[15b] Solutions were prepared by adding 1-2 drops of 50 mM (in 18 MΩ-cm H_2O) metal chloride (KCl, RbCl, or CsCl,) solution into a saturated TM9TP/acetonitrile solution. All solutions were injected at the rate of 120 μL h^{-1} into an Apollo II electrospray ionization (ESI) source. Ions were accumulated for between 1.0 s to 3.0 s in the hexapole ion accumulation cell prior to being transferred to the ICR cell. Prior to activation of the M(TM9TP) ions by SORI-CID, BIRD, or IRMPD, ions with the desirable mass were selected by standard FTICR techniques.

SORI-CID experiments were carried out by increasing the translational energy to a maximum of 1.5 eV (centre of mass) using a 500 Hz offset from the cyclotron frequency, and pulsing Ar into the ICR cell at a pressure of about 10^{-5} mbar for 250 ms. For BIRD experiments, the FTICR cell was heated to increase the internal energy of the ions by increasing the blackbody radiation field.[22d, 28] The magnet was protected from the heat source using a water-cooled heating jacket on the outside of the ICR cell vacuum tube.[29] Parent and fragment ion intensities were measured as a function of time.

IRMPD spectroscopy was done with a tunable OPO laser with a bandwidth of 2 cm^{-1} scanned from 2700 cm^{-1} to 3150 cm^{-1} in 2 cm^{-1} steps. Irradiation times were 1 s for $Cs(TM9TP)^+$ and 2 s for $Rb(TM9TP)^+$ at each wavelength. The OPO is built around a periodically-poled $LiNbO_3$ crystal which is pumped by a diode-pumped solid state Nd:YAG laser. The OPO operates at 20 kHz, with a pulse duration of a few nanoseconds and operated with an output power near 1 W at 3 μm.

Computational: B3LYP density functional theory was used for all geometry optimizations, frequency calculations, and electrostatic potential maps with the 6-31+g(d,p) basis set on C and H and with the Def2SVP basis set on Rb and Cs using the Gaussian 09 suite of programs and were corrected with the D3 dispersion correction.[30] Some calculations were repeated with the CAM-B3LYP set of functionals which incorporates a long range correction.[31] Calculated frequencies of $Rb(TM9TP)^+$ and $Cs(TM9TP)^+$ were scaled by 0.948. QST3, a synchronous transit-guided quasi-Newton (STQN) method, was used to search for the transition states from *endo*-$M(TM9TP)^+$ (M=K, Rb, and Cs) to *exo*-$M(TM9TP)^+$. Transition

states were characterized by an imaginary frequency involving the correct relative atomic motions.

Master Equation Modelling: The master equation is used to simulate energy changes in populations of the internal energy levels of a system over a period of time. A set of coupled linear first-order ordinary differential equations and the radiative absorption, emission, and dissociation rate constants of all state-to-state transitions are used to find the probability of energy transfer between all possible internal energy states. Once a Boltzmann distribution of ion populations and a steady-state is reached, the unimolecular decomposition rate constants can be obtained. To compute the dissociation and radiative rate constants, the computed vibrational frequencies and intensities were used for the *endo* and *exo* complexes. The Arrhenius pre-exponential factors depend on the looseness of the transition states. In the present case the transition states are expected to be neutral to loose, i.e. the transition state resembles the complex or, since it is dissociating, the transition state is more loose than the complex. To obtain transition state entropies, $\Delta S^{\neq}$, of between 0 and 50 J K^{-1} mol^{-1}—neutral to slightly loose—the computed vibrational frequencies of the complex are scaled by by a factor less than one. The master equation analysis done here was developed in the Williams lab.[32]

Acknowledgements

Financial support of this work from the Natural Sciences and Engineering Research Council (NSERC) of Canada (G.J.B., T.D.F.) is gratefully acknowledged. The Canada Foundation for Innovation (CFI), Industrial Research and Innovation Fund (IRIF), and Bruker are gratefully acknowledged for their support of the Laboratory for the Study of Gaseous Ion Structures, Energetics and Reactions (T.D.F.). Computational support from the Atlantic Computational Excellence Network (ACE-NET) and Western Canada Research Grid (West-Grid) is also gratefully acknowledged (T.D.F.). Y. Chen also extends gratitude to the China Scholarship Council. B.D. Linford is acknowledged for his technical help at the beginning of the research.

Keywords: cyclophane • host-guest complexes • IRMPD spectroscopy • mass spectrometry • blackbody infrared radiative dissociation

References

[1] Nobelprize.org. Nobel Media AB 2014. Web. .

[2] a) G. W. Gokel, W. M. Leevy, M. E. Weber, *Chem. Rev.* **2004**, *104*, 2723-2750; b) C. J. Pedersen, *Angew. Chem., Int. Ed. Engl.* **1988**, *27*, 1021-1027.

[3] a) E. Gazit, *Chem. Soc. Rev.* **2007**, *36*, 1263-1269; b) J. M. Lehn, *Angew. Chem., Int. Ed. Engl.* **1988**, *27*, 89-112; c) S. Mahdizadeh, G. Rounaghi, M. Mohajeri, F. Karimian, *Russ. J. Inorg. Chem.* **2016**, *61*, 791-798.

[4] a) D. J. Cram, *Angew. Chem., Int. Ed. Engl.* **1988**, *27*, 1009-1020; b) M.-J. Paik, J. S. Kang, B.-S. Huang, J. R. Carey, W. Lee, *J. Chromatogr. A* **2013**, *1274*, 1-5.

[5] J. L. Atwood, J. W. Steed, *Encyclopedia of Supramolecular Chemistry, Vol. 1*, CRC Press, **2004**.

[6] a) Y. Yuan, G. Gao, Z.-L. Jiang, J.-S. You, Z.-Y. Zhou, D.-Q. Yuan, R.-G. Xie, *Tetrahedron* **2002**, *58*, 8993-8999; b) K. Kano, T. Hayakawa, S. Hashimoto, *Bull. Chem. Soc. Jpn.* **1991**, *64*, 778-784; c) G. Cooke, V. M. Rotello, *Chem. Soc. Rev.* **2002**, *31*, 275-286; d) F. Biedermann, W. M. Nau, H. J. Schneider, *Angew. Chem., Int. Ed.* **2014**, *53*, 11158-11171; e) E. A. Meyer, R. K. Castellano, F. Diederich, *Angew. Chem., Int. Ed.* **2003**, *42*, 1210-1250; f) D. A. Dougherty, *Acc. Chem. Res.* **2012**, *46*, 885-893.

[7] F. Diederich, P. J. Stang, R. R. Tykwinski, *Modern Supramolecular Chemistry: Strategies for Macrocycle Synthesis*, John Wiley & Sons, **2008**.

[8] P. G. Ghasemabadi, T. Yao, G. J. Bodwell, *Chem. Soc. Rev.* **2015**, *44*, 6494-6518.

[9] a) F. Diederich, *Cyclophanes*, Royal society of chemistry: London, UK, **1991**; b) I. Pochorovski, F. Diederich, *Isr. J. Chem.* **2012**, *52*, 20-29.

[10] P. Rajakumar, M. Srisailas, *Tetrahedron Lett.* **2002**, *43*, 1909-1913.

[11] a) S. Bartoli, S. Roelens, *J. Am. Chem. Soc.* **2002**, *124*, 8307-8315; b) J. Yoon, S. K. Kim, N. J. Singh, K. S. Kim, *Chem. Soc. Rev.* **2006**, *35*, 355-360; c) C. Li, *Chem. Commun.* **2014**, *50*, 12420-12433.

[12] M. Arunachalam, I. Ravikumar, P. Ghosh, *J. Org. Chem.* **2008**, *73*, 9144-9147.

[13] S. J. Emond, P. Debroy, R. Rathore, *Org. Lett.* **2008**, *10*, 389-392.

[14] a) G. J. Bodwell, J. N. Bridson, T. J. Houghton, J. W. Kennedy, M. R. Mannion, *Angew. Chem.* **1996**, *108*, 1418-1420; b) G. J. Bodwell, J. N. Bridson, T. J. Houghton, J. W. Kennedy, M. R. Mannion, *Angew. Chem., Int. Ed. Engl.* **1996**, *35*, 1320-1321; c) G. J. Bodwell, J. N. Bridson, T. J. Houghton, J. W. Kennedy, M. R. Mannion, *Chem. - Eur. J.* **1999**, *5*, 1823-1827; d) G. J. Bodwell, J. J. Fleming, M. R. Mannion, D. O. Miller, *J. Org. Chem.* **2000**, *65*, 5360-5370; e) G. J. Bodwell, J. J. Fleming, D. O. Miller, *Tetrahedron* **2001**, *57*, 3577-3585; f) G. J. Bodwell, D. O. Miller, R. J. Vermeij, *Org. Lett.* **2001**, *3*, 2093-2096; g) G. J. Bodwell, J. N. Bridson, M. K. Cyrañski, J. W. Kennedy, T. M. Krygowski, M. R. Mannion, D. O. Miller, *J. Org. Chem.* **2003**, *68*, 2089-2098; h) B. Zhang, G. P. Manning, M. A. Dobrowolski, M. K. Cyranski, G. J. Bodwell, *Org. Lett.* **2008**, *10*, 273-276; i) M. A. Dobrowolski, M. K. Cyrański, B. L. Merner, G. J. Bodwell, J. I. Wu, P. v. R. Schleyer, *J. Org. Chem.* **2008**, *73*, 8001-8009; j) R. J. Vermeij, D. O. Miller, L. N. Dawe, I. Aprahamian, T. Sheradsky, M. Rabinovitz, G. J. Bodwell, *Aust. J. Chem.* **2010**, *63*, 1703-1716; k) Y. Yang, M. R. Mannion, L. N. Dawe, C. M. Kraml, R. A. Pascal Jr, G. J. Bodwell, *J. Org. Chem.* **2011**, *77*, 57-67; l) P. Kahl, J. P. Wagner, C. Balestrieri, J. Becker, H. Hausmann, G. J. Bodwell, P. R. Schreiner, *Angew. Chem.* **2016**, *128*, 9423-9427; m) B. Zhang, Y. Zhao, G. J. Bodwell, *Synlett* **2016**, *27*, 2113-2116.

[15] a) B. L. Merner, L. N. Dawe, G. J. Bodwell, *Angew. Chem., Int. Ed.* **2009**, *48*, 5487-5491; b) B. L. Merner, K. S. Unikela, L. N. Dawe, D. W. Thompson, G. J. Bodwell, *Chem. Commun.* **2013**, *49*, 5930-5932.

[16] a) A. P. Bisson, V. M. Lynch, M. K. C. Monahan, E. V. Anslyn, *Angew. Chem., Int. Ed. Engl.* **1997**, *36*, 2340-2342; b) F. Diederich, K. Dick, *J. Am. Chem. Soc.* **1984**, *106*, 8024-8036; c) J. Forman, R. Marsh, W. Schaefer, D. Dougherty, *Acta Crystallogr., Sect. B: Struct. Sci.* **1993**, *49*, 892-896; d) J. A. Gavin, N. Deng, M. Alcalá, T. E. Mallouk, *Chem. Mater.* **1998**, *10*, 1937-1944; e) Y. A. Zhelezina, A. S. Balueva, S. N. Ignatieva, A. A. Karasik, O. G. Sinyashin, *Phosphorus, Sulfur Silicon Relat. Elem.* **2013**, *188*, 19-20.

[17] a) C. A. Schalley, *Int. J. Mass Spectrom.* **2000**, *194*, 11-39; b) C. A. Schalley, *Analytical Methods in Supramolecular Chemistry: Vol. 1*, **2012**.

[18] E. Warneke, C. Jenne, J. Bernarding, V. A. Azov, M. Plaumann. *Chem. Commun*. **2016,** *52*, 6300.

[19] P. Hurtado, F. Gámez, S. Hamad, B. Martínez-Haya, J. D. Steill, J. Oomens. *J. Phys. Chem. A*. **2011**,*115*, 7275.

[20] T. E. Cooper, D. R. Carl, J. Oomens, J. D. Steill, P. B. Armentrout *J. Phys. Chem. A.* **2011**, *115*, 5408.

[21] B. Martínez-Haya, P. Hurtado, A. R. Hortal, S. Hamad, J. D. Steill, J. Oomens. *J. Phys. Chem. A*. **2010**, *114*, 7048.

[22] a) M. Azargun, Y. Jami-Alahmadi, T. Fridgen, *Phys. Chem. Chem. Phys.* **2017**, *19*, 1281-1287; b) E. A. Gillis, M. Demireva, M. G. Sarwar, M. G. Chudzinski, M. S. Taylor, E. R. Williams, T. D. Fridgen, *Phys. Chem. Chem. Phys.* **2013**, *15*, 7638-7647; c) *Science* **1998**, *279*, 149b-149b; d) R. C. Dunbar, T. B. McMahon, D. Tholmann, D. S. Tonner, D. R. Salahub, D. Wei, *J. Am. Chem. Soc.* **1995**, *117*, 12819-12825.

[23] D. Thoelmann, D. S. Tonner, T. B. McMahon. *J. Phys. Chem.* **1994**, *98*, 2002.

[24] K. Hiraoka, E. P. Grimsrud, and P. Kebarle. *J. Am. Chem. Soc*. **1974**, *96*, 3359.

[25] M. Meot-Ner, C. V. Speller. *J. Phys. Chem.* **1986**, *90*, 6616.

[26] a) T. D. Fridgen, *Mass Spectrom. Rev.* **2009**, *28*, 586-607; b) N. C. Polfer, J. Oomens, *Mass Spectrom. Rev.* **2009**, *28*, 468-494; c) M. Burt, T. Fridgen, *Eur. J. Mass Spectrom.* **2012**, *18*, 235.

[27] a) M. B. Burt, T. D. Fridgen. *J. Phys. Chem. A*, **2007**, 111, 10738; b) T. D. Fridgen, L. MacAleese, P. Maitre, T. B. McMahon, P. Boissel, J. Lemaire *Phys. Chem. Chem. Phys*., **2005**,7, 2747; c) J. R. Roscioli, L. R. McCunn, M. A. Johnson, *Science,* **2007**, 316, 249.

[28] W. D. Price, P. D. Schnier, E. R. Williams, *J. Phys. Chem. B* **1997**, *101*, 664-673.

[29] K. Rajabi, M. L. Easterling, T. D. Fridgen, *J. Am. Soc. Mass Spectrom.* **2009**, *20*, 411-418.

[30] M. J. Frisch, G. W. Trucks, H. B. Schlegel, G. E. Scuseria, M. A. Robb, J. R. Cheeseman, G. Scalmani, V. Barone, B. Mennucci, G. A. Petersson, H. Nakatsuji, M. Caricato, X. Li, H. P. Hratchian, A. F. Izmaylov, J. Bloino, G. Zheng, J. L. Sonnenberg, M. Hada, M. Ehara, K. Toyota, R. Fukuda, J. Hasegawa, M. Ishida, T. Nakajima, Y. Honda, O. Kitao, H. Nakai, T. Vreven, J. A. Montgomery Jr., J. E. Peralta, F. Ogliaro, M. J. Bearpark, J. Heyd, E. N. Brothers, K. N. Kudin, V. N. Staroverov, R. Kobayashi, J. Normand, K. Raghavachari, A. P. Rendell, J. C. Burant, S. S. Iyengar, J. Tomasi, M. Cossi, N. Rega, N. J. Millam, M. Klene, J. E. Knox, J. B. Cross, V. Bakken, C. Adamo, J. Jaramillo, R. Gomperts, R. E. Stratmann, O. Yazyev, A. J. Austin, R. Cammi, C. Pomelli, J. W. Ochterski, R. L. Martin, K. Morokuma, V. G. Zakrzewski, G. A. Voth, P. Salvador, J. J. Dannenberg, S. Dapprich, A. D. Daniels, Ö. Farkas, J. B. Foresman, J. V. Ortiz, J. Cioslowski, D. J. Fox, Gaussian, Inc., Wallingford, CT, USA, **2009**.

[31] T. Yanai, D. P. Tew, N. C. Handy, *Chemical Physics Letters* **2004**, *393*, 51-57.

[32] a) W. D. Price, P. D. Schnier, E. R. Williams, *Anal. Chem.* **1996**, *68*, 859-866; b) E. A. Gillis, M. Demireva, K. Nanda, G. Beran, E. R. Williams, T. D. Fridgen, *Phys. Chem. Chem. Phys.* **2012**, *14*, 3304-3315.

Entry for the Table of Contents (Please choose one layout)

Layout 1:

FULL PAPER

Text for Table of Contents

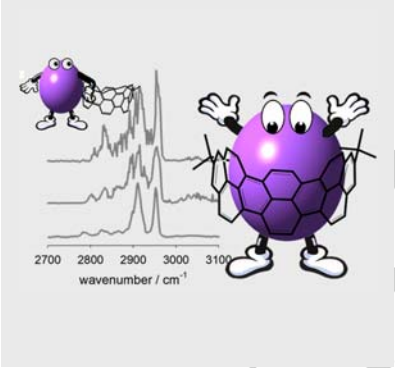

*Author(s), Corresponding Author(s)**

Page No. – Page No.

Title

Layout 2:

FULL PAPER

((Insert TOC Graphic here; max. width: 11.5 cm; max. height: 2.5 cm))

*Author(s), Corresponding Author(s)**

Page No. – Page No.

Title

Text for Table of Contents